Topological Homogeneity for Electron Microscopy Images

Helena Molina-Abril[1], Fernando Diaz del Rio[1], Maria P. Guerrero-Lebrero[2], Pedro Real[1], Guillermo Barcena[2], Veronica Braza[3], Elisa Guerrero[2], David Gonzalez[3], and Pedro L. Galindo[2]

[1] H.T.S. Informatics' Engineering, University of Seville, Seville, Spain
habril@us.es
[2] Department of Computer Science and Engineering, University of Cadiz, 11510 Puerto Real, Cadiz, Spain
[3] University Research Institute on Electron Microscopy and Materials (IMEYMAT), University of Cadiz, 11510 Puerto Real, Cadiz, Spain

Abstract. In this paper, the concept of homogeneity is defined, from a topological perspective, in order to analyze how uniform is the material composition in 2D electron microscopy images. Topological multiresolution parameters are taken into account to obtain better results than classical techniques.

Keywords: Topology · Homogeneity · Electron microscopy · Images

1 Introduction

Microscopy imaging techniques are employed by scientists and researchers to improve their ability to view the microscopic world. The obtained 2D images are used to get information about structure and/or composition distributions of the studied objects and one of the parameters to be usually required is the analysis of the homogeneity. Certainly, the two-dimensional homogeneity question crops up in many different scientific fields. Thus, in quality assurance programs, surface smoothness may be checked in different blocks of material. In biological investigations, the density of a biological tissue may be recorded for purposes of detecting regions of different contrasts [1]. In material science, electron microscopy images are used to evaluate the elemental distribution or strain fields in order to characterize its structure.

In all these situations, the same issue arises. Given a two-dimensional matrix of measurements, it is necessary to assess the randomness [2], the apparition of patterns or microstructure, the lack of gradients, etc. in the image. The formulation of this question overlooks any concept of a formal statistical distribution [5].

This work has been supported by the Spanish research projects MTM2016-81030-P, TEC2012-37868-C04-02 (AEI/FEDER, UE) and the VPPI of the University of Seville.

The question is not how to characterize in a probabilistically way the observations [3,4]; rather it is to characterize how observations could relate with each other locally. In this paper, the concept of homogeneity is defined, from a topological perspective, in order to analyze the homogeneity in 2D electron microscopy images. Topological multiresolution parameters are taken into account to obtain better results than classical techniques.

2 Electron Microscopy Image Data

In recent years, GaAsSbN alloys have been established as an effective material for solar cell applications. To solve the problems that are recurrent in quaternary alloys, a new approach has been adopted by means of the growth of superlattice (SL) structures. These SL structures consists in very thin layers epitaxially grown that could give supplementary advantages over bulk counterparts, such as an extra bandgap tunability via period thickness or better crystal qualities.

In this work, two SL structures have been studied before and after an annealing at 800 °C: type-I (GaAsSbN/GaAs) and type-II (GaAsSb/GaAsN) grown over a GaAs substrate. HAADF and LAADF images were simultaneously acquired in STEM mode in a double aberration corrected FEI Titan3 Cubed Themis operated at 200 kV and used to obtain distribution maps of N from a methodology through the suitable normalization and discrimination of the intensity ratios of HAADF and LAADF images [12]. Figure 1 shows these calculated N mappings where (a) and (b) belong to type-I SL images (before and after RTA process respectively) and (c) and (d) correspond to type-II SL images.

These mappings are built to characterize the distribution of N inside these SL and find its relationship with the photoluminescence and photocurrent properties. Ideally, N should incorporate in a square-wave profile with a constant and homogeneous composition obtained by random distribution of N in V-sites. However, N competes for these lattice positions with As and Sb so there are serious difficulties in the precise control of the Sb and N contents [7,11]. In addition, the extremely low solubility of N in these alloys could favors the formation of N-rich regions [10,13,16]. All of this suggests that the growth of high quality III-V-N structures may be difficult to achieve [7,8,14]. Several approaches has been proposed to overcome these issues. On one hand, it is suggested the spatial separation of Sb and N atoms as in type-II SL could avoid the ubiquitous growth problems during the simultaneous growth of Sb and N that happens in type-I improving crystal quality [9]. On the other hand, it is believed that post-growth annealing processes may also increase the homogeneity of N within the layer by decreasing composition fluctuations. In addition, device performance is a strong function of the quality of the interfaces. The formation of atomically flat interfaces by suppressing surface undulations is fundamental to enhance their optical properties [6,15]. In each case, to check the possible improvements of the crystal quality, it is necessary to compare and evaluate both approaches and the effect of the thermal annealing in terms of homogeneity.

The study of homogeneity, among others, could determine this closeness/distance of the ideal design. Until now, to calculate the homogeneity of

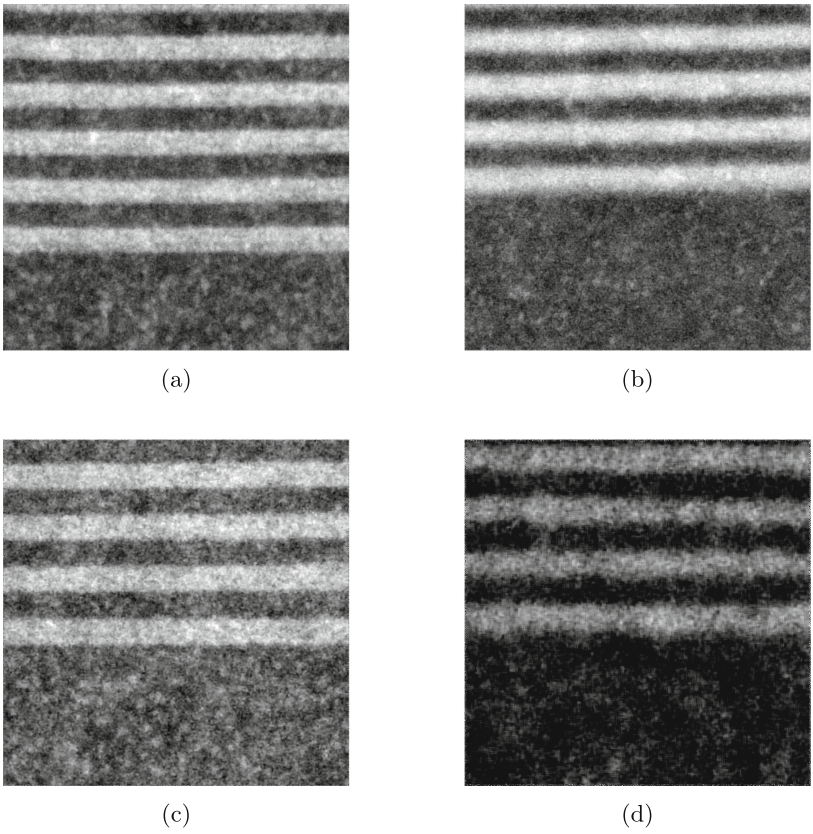

Fig. 1. Mappings of the N distribution of type-I (a) and type-II (c) as grown and after annealing (b) y (d), respectively. We used a grey scale, where white is indicative of the highest N content and black of the lowest one.

these images, the standard deviation of the values has been used to estimate it. The higher the standard deviation, the lower the homogeneity. However, this procedure is too simple for 2D analyses, as they do not take into account the possibility of regular gradients or patterns that may add a certain degree of symmetry or order to the material, the presence or degree of clusters as well as the abruptness or roughness of the interfaces. Considering all this, it seems necessary to use topological techniques to define homogeneity in order to obtain better results.

3 Related Works

Current methods dealing with the problem of measuring how far a given material is from a constant composition, clearly fail when trying to analyze the homogeneity of 2D electron microscopy images.

Linear homogeneity measures have been used in some cases for some simple images. For example, the mean and standard deviation of the gray frequency histogram can give an approximate idea of the two-dimensional homogeneity when the set of images are very different in gray levels. However, for the general case these simple values are not relevant at all. Some plain examples illustrate this issue. Let us consider two 256×256 images with very different "homogeneity aspects". Firstly, a chessboard-like image with interlaced values of 0 and 255, and secondly an image with two parts: one is pure black (0) and the other pure white (255). Neither arithmetic mean nor standard deviation provide distinction at all among these extreme cases (they are 127.500 and 127.501 resp.). We are conscious that the concept of "homogeneity" is being intuitively expressed by now, but the difference between both images obvious. Another almost homogeneous image where mean and deviation return paradoxically high values is an image where each row has the gray level of the precedent plus one (in our case, 256 rows with grey from 0 to 255). In this case, mean results also in 127.500 and deviation in 73.901. Hence, it is clear that simple measures are not valid to express the homogeneity of grey level images.

Here we present a topology-based method, in which standardized topological numbers provide a robust quantity for measuring how uniform is the material composition.

There have been another more sophisticated attempts in using digital topology for measuring image's homogeneity. One of the first one was presented in [19]. However, authors there did not provide a quantity for comparing homogeneity among images, but a multiresolution representation that can be used for texture characterization. More recent methods dealing with texture classification can be seen in [17,20]. These works deal with texture classification by applying machine learning algorithms to a set of features obtained from the image. Other more complicated functionals have also been proposed for comparing noisy experimental image data with statistical models (see [18]). However, to the best of our knowledge, there are no results satisfying that: (1) Have been successfully applied to Electron Microscopy Image data, and (2) provide a normalized homogeneity measure for image comparison.

4 Topological Techniques

Let us first recall basic notions in the field of digital images and digital topology. We denote by $\mathbb{Z}$ the set of relative integers. A point $x \in \mathbb{Z}^2$ is defined by (x_1, x_2) with $x_i \in \mathbb{Z}$. A 2D grayscale image may be seen as a map $\mathcal{I}$ from $\mathbb{Z}^2$ to $\mathbb{Z}$. For each point $x \in \mathbb{Z}^2$, $\mathcal{I}(x)$ is the (graylevel) intensity value of x. A binary 2D image is then seen as the map $\mathcal{B}$ from $\mathbb{Z}^2$ to $\{0, 1\}$.

For each point (pixel) in a given 2D image, we consider two local adjacency relations Γ_4 and Γ_8 defined: For each point $x \in \mathbb{Z}^2$:

$$\Gamma_4(x) = \{y \in \mathbb{Z}^2; |y_1 - x_1| + |y_2 - x_2| \leq 1\}$$

$$\Gamma_8(x) = \{y \in \mathbb{Z}^2; max(|y_1 - x_1|, |y_2 - x_2|) \leq 1\}$$

In the following, we will denote by n a number such that $n = 4$ or $n = 8$. We define $\Gamma_n^*(x) = \Gamma_n(x) \backslash \{x\}$. The point $y \in \mathbb{Z}^2$ is n-adjacent to $x \in \mathbb{Z}^2$ if $y \in \Gamma_n(x)$.

In this section, electron microscopy images will be analyzed from a topological point of view, by first of all, creating their corresponding so called "crack images". Crack images are binary images created by considering each possible gray level difference among adjacent pixels. That is, if the gray-scale of image $\mathcal{I}$ is composed by G gray levels, we will create $G-1$ binary crack images for image $\mathcal{I}$ (plus an initial gray scale image denoted as $\mathcal{I}_0^{Crk}$). From now on, the number of possible gray levels in a given image $\mathcal{I}$ will be denoted as G, and the different levels of gray that are actually present in $\mathcal{I}$ will be denoted as $g_1, \ldots g_l$. In the following Figures with binary images, value zero will be represented in black color, and value one in white color.

First of all, if $\mathcal{I}$ is a $(Nrows \times Ncols)$ image, a new gray-scale image $\mathcal{I}_0^{Crk}$ with $((2*Nrows+1) \times (2*Ncols+1))$ pixels is created by adding a black frame of width 1 surrounding the original image, and adding a new pixel between each pair of 4-adjacent pixels in $\mathcal{I}$. All these added pixels are set to the following values: Pixels belonging to the frame surrounding the original image are set to zero, and will be denoted as $\mathcal{F}$. Pixels added between each pixel in $\mathcal{I}$ are set to one. These pixels in $\mathcal{I}_0^{Crk}$ will be denoted as $\mathcal{A}$. All the other pixels (the ones corresponding to the original image) are set to their corresponding value in $\mathcal{I}$ and will be denoted as $\mathcal{O}$. Figure 2(a) shows a synthetic image whose gray-scale contains 6 levels that are all of them present in the image ($G = 6$, $l = 6$, $g_1 = 0$ and $g_6 = 5$). An example of its corresponding $\mathcal{I}_0^{Crk}$ image is depicted in Fig. 2(b), where $\mathcal{F}$ are set to zero, $\mathcal{A}$ are set to one and $\mathcal{O}$ are set to their original values. Then, for the construction of the corresponding crack images, the gray level will be used as a threshold for checking intensity differences among each 4-adjacent pixel in the original image.

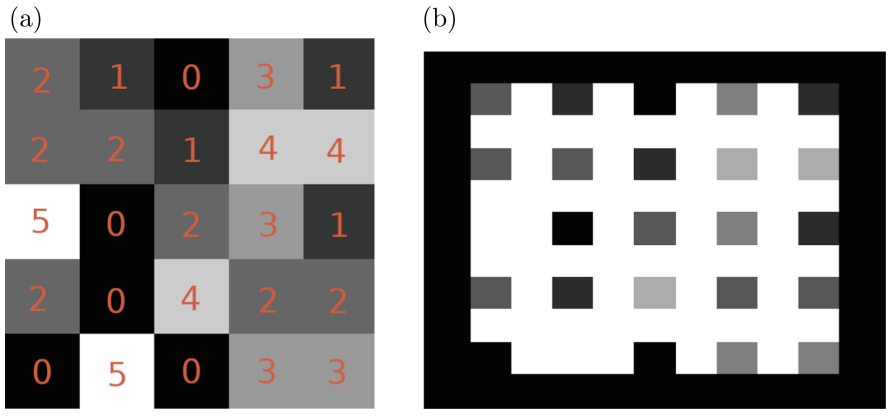

Fig. 2. (a) Synthetic image $\mathcal{I}$ showing different gray intensities and (b) its corresponding $\mathcal{I}_0^{Crk}$

Algorithm 1 shows the process of crack images generation. The main idea here, is that for each possible gray-value difference d, the corresponding crack image $\mathcal{I}_d^{Crk}$ represents fissures separating image regions whose gray-level difference is above (or equal to) this quantity d.

Algorithm 1. [Creating crack images]

Input: A digital 2D Image $\mathcal{I}$ in a gray-scale of G values

Generate $\mathcal{I}_0^{Crk}$, and define pixels in $\mathcal{A}$ and pixels in $\mathcal{O}$

for $d = 1$ to G **do**

for each point $x \in \mathcal{A}$ **do**

if $\exists\ y, z \in \Gamma_4^*(x) : y, z \in \mathcal{O}$ and $|\mathcal{I}_0^{Crk}(y) - \mathcal{I}_0^{Crk}(z)| >= d$ **then**

$I_d^C(x) = 0$

for each point $x \in \mathcal{A}$ **do**

if $\exists\ y, z \in \Gamma_4^*(x) : y, z \in \mathcal{A}$, $\mathcal{I}_d^{Crk}(y) = 0$ and $\mathcal{I}_d^{Crk}(z) = 0$ **then**

$\mathcal{I}_d^{Crk}(x) = 0$

for each point $x \in \mathcal{O}$ **do**

$n_0 = \#\{y \in \Gamma_8^*(x) : \mathcal{I}_d^{Crk}(y) = 0\}$

$n_1 = \#\{y \in \Gamma_8^*(x) : \mathcal{I}_d^{Crk}(y) = 1\}$

if $n_0 > n_1$ **then**

$\mathcal{I}_d^C(x) = 1$

else

$\mathcal{I}_d^C(x) = 0$

Output: A set of G crack images $\mathcal{I}_d^{Crk}$

The corresponding crack images for the synthetic image in Fig. 2(a) are shown in Fig. 3(a) to (e) for $d = 1$, $d = 2$, $d = 3$, $d = 4$ and $d = 5$ respectively. Note that at the beginning of the algorithm, all the pixels inserted between two pixels of the original image (denoted as $\mathcal{A}$) are set to one in $\mathcal{I}_0^{Crk}$. Taking for instance $d = 1$, and following Algorithm 1 the intensity difference among pixels is almost always greater or equal to one, so most of the added pixels will change their value to zero, giving as a result the image shown in Fig. 3(e) in which only six of these added pixels remain unchanged (value equal to one, colored in white).

Once a crack image is created for each gray-level difference, the number of connected black and connected white components are computed for each one of them. These numbers, corresponding to the well known Betti numbers of dimension 0 and 1 respectively, will be used a signature of the original image homogeneity. More exactly, the normalized sum of these Betti numbers along the gray spectrum is going to be demonstrated as a very robust measure of real image homogeneity. From now on, these sums will be referred here as B_0 (for the black components) and B_1 (for the white components).

The computation of a normalized sum of the well-known Euler number along the gray spectrum, i.e. $B_1 - B_0$ in our notation, is shown in Algorithm 2. The resulting value will be the homogeneity index for the analyzed images. Figure 3(f), shows the evolution of β_0 and β_1 with the progress of Algorithm 2

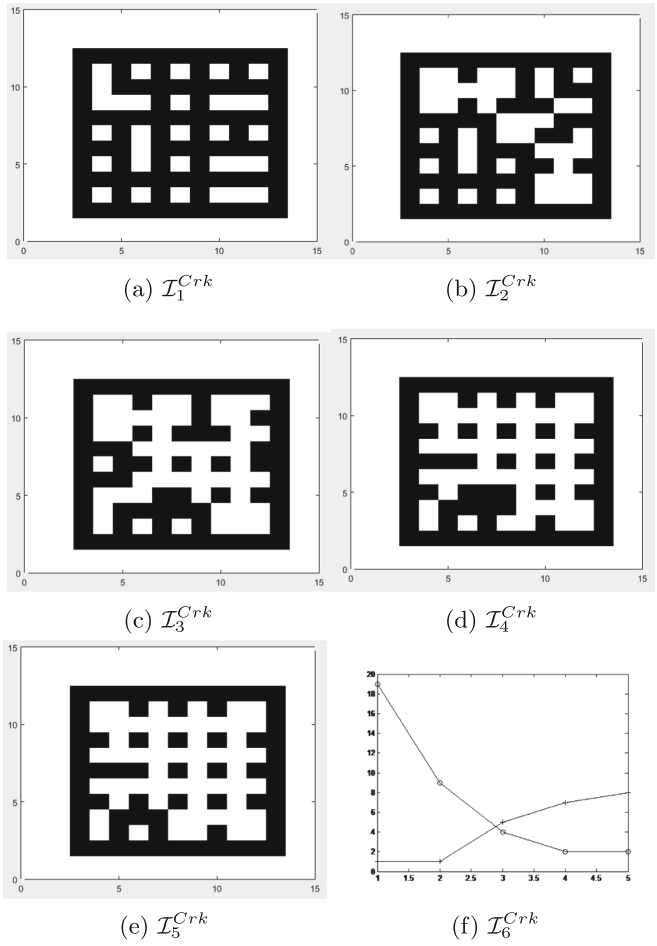

(a) $\mathcal{I}_1^{Crk}$ (b) $\mathcal{I}_2^{Crk}$

(c) $\mathcal{I}_3^{Crk}$ (d) $\mathcal{I}_4^{Crk}$

(e) $\mathcal{I}_5^{Crk}$ (f) $\mathcal{I}_6^{Crk}$

Fig. 3. Crack images corresponding to image in Fig. 2(a) and the evolution of homogeneity measures along all the possible gray differences. The line with crosses represents the β_0 whereas line with circles the β_1

(with d going from 1 to 5) for Image in Fig. 2(a). The evolution of β_0 is represented with crosses, and the evolution of β_1 with circles in the image.

According to previous construction of the crack images and homogeneity measures, it is interesting to observe the behavior of extremal (homogeneous vs. heterogeneous) images. Those images have the biggest and smallest $B_1 - B_0$ values respectively. These values, will be used for normalizing our B_0 and B_1 measures, so at the end, $-1 \leq B_1 - B_0 \leq 1$. On one hand, given a pure homogeneous image (of any gray constant level), all its crack images are the same (differing in size) as the one shown in Fig. 4(a). Analyzing β_0 and β_1 in these crack images, we will obtain the maximum number of connected black

Algorithm 2. [**Computing the homogeneity measure**]

Input: A set of $\mathcal{I}_d^{Crk}$ Crack Images

$B_0 = 0, B_1 = 0$
for $d = 1$ to G **do**
$\beta_0 =$ Betti number of dimension 0 of $\mathcal{I}_d^{Crk}$
$\beta_1 =$ Betti number of dimension 1 of $\mathcal{I}_d^{Crk}$
$B_0 = B_0 + \beta_0$
$B_1 = B_1 + \beta_1$
$B_0 = Normalize(B_0)$
$B_1 = Normalize(B_1)$
Output:$B_1 - B_0$

components β_0 and only one connected white component β_1. Note that the surrounding black frame inserts a black component that "touches" all the components in the four image borders, thus the number of maximum connected black components in the crack images is $1+(Nrows-2)*(Ncols-2)$, and the number of maximum connected white components is $(Nrows)*(Ncols)$, where $Nrows$ and $Ncols$ are the number of rows and columns of the original image. In the same way, the minimum number of connected black components and connected white components is one. Therefore, the crack image shown in Fig. 4(a) corresponding to a 5×5 homogeneous image, has $\beta_0 = 10$ and $\beta_1 = 1$.

On the other hand, Fig. 4(b) depicts the crack image for the maximum possible heterogeneous 5×5 image: a chessboard-like image with interlaced gray values of g_1 and g_l. All the possible crack images for gray-level differences in the range $[1, (g_l - g_1)]$ result in the same form (that of Fig. 4(b)), thus having the maximum number of white components (5×5 in this case) but only one black component. Therefore, the crack image shown in Fig. 4(b) has $\beta_0 = 1$ and $\beta_1 = 25$.

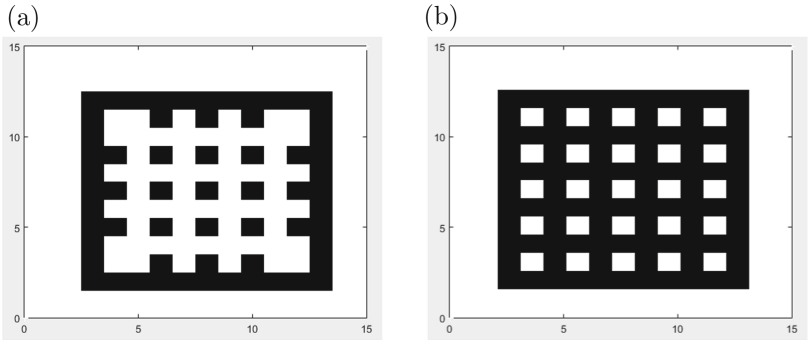

Fig. 4. (a) Crack image corresponding a homogeneous image. (b) Crack image corresponding to a heterogeneous chess-like image.

Thus, summing up β_0 and β_1 for any possible gray difference, in the case of an homogeneous image, B_1 has the minimum value $(G-1)$ (the result of summing up $G-1$ times the value one for $\beta_1 = 1$), and B_0 has the maximum value $(G*(1+(Nrows-2)*(Ncols-2)))$ where G is the number of possible gray-levels in the original image. Therefore, the normalization of our homogeneity measure B_1-B_0 will be commputed by dividing B_0 by $(G*(1+(Nrows-2)*(Ncols-2)))$ and B_1 by $(G*((Nrows)*(Ncols)))$. Doing that, we obtain $B_1 - B_0 = 1$ for a purely heterogeneous image (a chessboard-like image with interlaced extreme gray values) and $B_1 - B_0 = -1$ for a purely homogeneous image.

5 Experimentation

The relation between parameter $B_1 - B_0$ and homogeneity can be demonstrated by analyzing random synthetic images with different maximum and minimum gray levels. It is expected that those images with bigger gray contrasts between their pixels will be more heterogeneous, whereas the images with similar gray levels will present a high degree of homogeneity. Besides it is also required for a good homogeneity parameter that the size of the image has no influence on its value.

Table 1 shows the homogeneity results for different random gray-scale 28×28 images in which the maximum grey level has been modified. Figure 5 shows the evolution of the number of holes and connected components when the contrast is increased for the crack images of two synthetic random images. As stated in previous section, the more contrast the crack image has, the more connected components appear (that is, bigger β_0) and the less holes are found (i.e., smaller β_1). It is worth to mention that the size of the image has a negligible influence on the homogeneity values (slight variations because of the random generation of the images). Therefore, we can conclude that the bigger $B_1 - B_0$ is, the more heterogeneous the image is. No doubt that this analysis is far obvious for simple images like those presented in Sect. 3 (chessboard-like image, an image with a half part of pure black color and other in pure white, etc.).

Table 1. Homogeneity results for random 28×28 images varying the maximum gray difference

Maximum grey level	$B_1 - B_0$
10	−0.9735
50	−0.8645
100	−0.7257
150	−0.5883
200	−0.4655
255	−0.2908

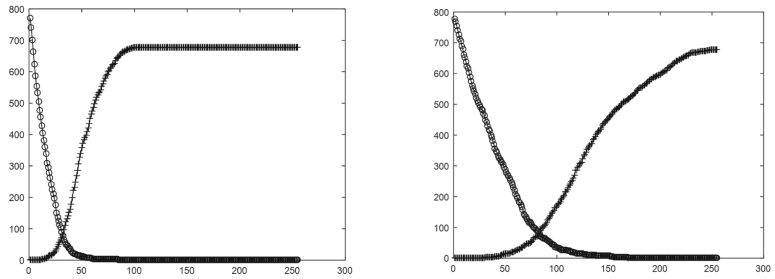

Fig. 5. (a) Representation of the number of holes and connected components vs. grey level for the crack images of two synthetic random images with maximum gray intensities of 100 (Left) and 255 (Right). The line with crosses represents the β_0 whereas line with circles the β_1

Experimentation has been carried out using images described in Sect. 2. Four of these images are shown in Fig. 1. Three samples of 100×100 pixels belonging to the white bands have been taken for each image (see Fig. 6 where samples (a) correspond to Fig. 1(a), samples (b) to Fig. 1(b), etc.).

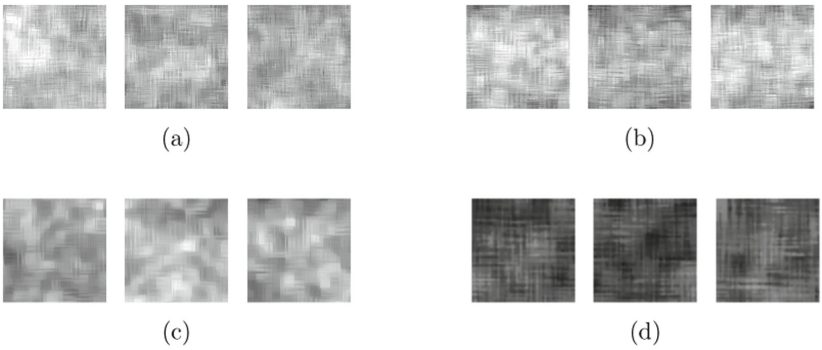

Fig. 6. Electron microscopy samples corresponding to images in Fig. 1

The resulting homogeneity measure $B_1 - B_0$ is shown in Table 2. As we can see, $B_1 - B_0$ values are very similar for any fragment extracted for the same image (around -0.960 for image (a), around -0.950 for image (b), around -0.976 for image (c) and around -0.972 for image d). More exactly, means for the three segments of images (a), (b), (c) and (d) are -0.9600, -0.9497, -0.9762, -0.9719, whereas standard deviation results to be 0.0007, 0.0006, 0.0006, 0.0010. This clearly points out the robustness of the proposed homogeneity measure $B_1 - B_0$.

Besides, the resemblance of all $B_1 - B_0$ values and their proximity to -1.0 indicate that the white bands are very homogeneous for all the tested electronic microscopy images. In fact, image histograms reveal that more than 95% of the

pixels have less than 100 different gray levels. In order to distinguish more clearly and with divergent measures these specific microscopy images, one can extend the normalized sum of the Euler numbers to a narrower range. The range $[1, 50]$ is discovered to represent more than 99% of all the possible contrasts (that is, β_0 reaches a value bigger than the 99% of its maximum). Computing the $B_1 - B_0$ for this reduced range we obtain Table 3.

As discussed in Sect. 3, we find also for these 4 images that the parameter $B_1 - B_0$ has any relation neither with the standard deviation nor with the mean. In Table 4 these linear values are presented for these images in order to corroborate that they would arrange the images in a completely different order than $B_1 - B_0$ would.

Finally, we can conclude for the microscopy images that they can be arranged with respect to their homogeneity in this order (from smaller to bigger): b, a, d, c. This parameter is currently helping microscopy imaging experts to analyze how thermal processes affect the structure and/or composition of different material.

In future works we expect that the homogeneity parameter described here, being a well defined and robust measure, would serve to analyze other images where texture and regularity play an important role, like those of skin cancer, granulometry, porosity materials, etc.

Table 2. Homogeneity results for samples in Fig. 6

	Image (a) $B_1 - B_0$	Image (b) $B_1 - B_0$	Image (c) $B_1 - B_0$	Image (d) $B_1 - B_0$
Sample 1	−0.9603	−0.9504	−0.9769	−0.9708
Sample 2	−0.9592	−0.9495	−0.9759	−0.9723
Sample 3	−0.9605	−0.9492	−0.9758	−0.9727

Table 3. Homogeneity results for samples in Fig. 6 in the range [1, 50]

	Image (a) $B_1 - B_0$	Image (b) $B_1 - B_0$	Image (c) $B_1 - B_0$	Image (d) $B_1 - B_0$
Sample 1	−0.7651	−0.7172	−0.8467	−0.8166
Sample 2	−0.7598	−0.7128	−0.8416	−0.8242
Sample 3	−0.7665	−0.7113	−0.8413	−0.8261

Table 4. Standard deviation and mean for samples in Fig. 6

	Image (a)	Image (b)	Image (c)	Image (d)
Standard deviation	45.0804	45.1256	37.4100	27.7506
Mean	194.4156	189.1598	159.2374	92.0668

6 Conclusions

In this paper, the concept of homogeneity is defined, from a topological perspective, in order to analyze the homogeneity in 2D electron microscopy images. A standardized topological number is provided as a robust quantity for measuring how uniform is the material composition.

The proposed topological number has been applied to numerically analyze the homogeneity of nitrogen distribution in composition maps obtained from ADF STEM images in type I (GaAsSbN/GaAs) and type II (GaAsSb/GaAsN) superlattice structures before and after RTA. A range of homogeneity between the samples has been established. First, it is shown that the SL-I image gives a parameter $B_1 - B_0$ higher than the SL-II. Secondly, our calculations show that annealing treatment results in a significant increase in uniformity in both types of SLs, i.e. better diffusion leads to a homogenization of the distribution of N within the layer. Our analysis has revealed that this increase during RTA is higher in SL-II than in SL-I and this result is in agreement with the photoluminescence results.

Further work extending this measure to higher dimensions and considering other more sophisticated topological relations will be performed in the future. Extensions to other possible applications in which homogeneity measures might be useful will be assessed as well (biomedical, astronomical images, etc.).

References

1. Miller, R.L., Kahn, J.S.: Statistical Analysis in the Geological Sciences. Wiley, New York (1962)
2. Yaglom, A.M.: An Introduction to the Theory of Stationary Random Functions. Prentice Hall, Englewood Cliffs (1962)
3. Materm, B.: Spatial variation. Comm. Swed. For. Res. Inst. **49**, 144 (1960)
4. Ripley, B.: Spatial Statistics. Wiley, New York (1981)
5. Cramer, H., Leadbetter, M.R.: Stationary and Related Stochastic Processes. Wiley, New York (1967)
6. Ahsan, N., Miyashita, N., Islam, M., Yu, K., Walukiewicz, W., Okada, Y.: Effect of Sb on GaNAs intermediate band solar cells. IEEE J. Photovoltaics **3**(2), 730–736 (2013)
7. Braza, V., et al.: Sb and N incorporation interplay in GaAsSbN/GaAs Epilayers near lattice-matching condition for 1.0–1.16-eV photonic applications. Nanoscale Res. Lett. **12**(1), 356 (2017)
8. Cheah, W.K., Fan, W.J., Wicaksono, S., Yoon, S.F., Tan, K.H.: Low antimony-doped GaNxAs1-x on GaAs grown by solid-source molecular-beam epitaxy. J. Cryst. Growth **254**(3–4), 305–309 (2003)
9. Gonzalo, A., et al.: Strain-balanced type-II superlattices for efficient multi-junction solar cells. Sci. Rep. **7**(1), 4012 (2017)
10. Ho, I.H., Stringfellow, G.B.: Solubility of nitrogen in binary III–V systems. J. Cryst. Growth **178**(1–2), 1–7 (1997)
11. Reyes, D.F., et al.: Modelling of the Sb and N distribution in type II GaAsSb/GaAsN superlattices for solar cell applications. Appl. Surf. Sci. **442**, 664–672 (2018)

12. Ruiz-Marin, N., et al.: Nitrogen mapping from (HA) ADF analysis in quaternary dilute nitride superlattices 1 introduction. Appl. Surf. Sci. (in Review)
13. Stringfellow, G.B.: Thermodynamic considerations for epitaxial growth of III/V alloys. J. Cryst. Growth **468**, 11–16 (2017)
14. Wu, L.J., et al.: MBE growth and properties of GaAsSbN/GaAs single quantum wells. J. Cryst. Growth **279**(3–4), 293–302 (2005)
15. Wu, Z.H., et al.: Spontaneous formation of highly regular superlattice structure in InGaN epilayers grown by molecular beam epitaxy. Appl. Phys. Lett. **98**(14), 4–7 (2011)
16. Zhang, S.B., Wei, S.H.: Nitrogen solubility and induced defect complexes in epitaxial GaAs:N. Phys. Rev. Lett. **86**(9), 1789–1792 (2001)
17. Barros Neiva, M., Vacavant, A., Martinez Bruno, O.: Improving texture extraction and classification using smoothed morphological operators. Digit. Sig. Process. **83**, 24–34 (2018)
18. Mantz, H., Jacobs, K., Mecke, K.: Utilizing Minkowski functionals for image analysis: a marching square algorithm. J. Stat. Mech. Theory Exp. **12**, 12015 (2008)
19. Pikazi, A., Averbuch, A.: An efficient topological characterization of gray-levels textures, using a multiresolution representation. Graph. Models Image Process. **59**(1), 1–17 (1997)
20. Sonali Dash, S., Ranjan Jena, U.: Multi-resolution Laws' Masks based texture classification. J. Appl. Res. Technol. **15**, 571–582 (2018)